International Journal of Academic Engineering Research (IJAER)
ISSN: 2643-9085
Vol. 8 Issue 5 May - 2024, Pages: 1-10

Enhancing the Transient Response of Induction Motor Using Double Cage Rotor Model

I. M. Uneze1, I. U. Uju2, C. O. Uneze3

1Department of Electrical and Electronics Engineering
Imo State Polytechnic
Omuma, Nigeria
2Department of Electrical and Electronics Engineering
Chukwuemeka Odumegwu Ojukwu University
Uli, Nigeria
3Department of Software Engineering
Federal University of Technology Owerri
Owerri, Nigeria

Abstract: *A 37.3 kW single-cage motor has been modelled and then upgraded to a double-cage rotor via modelling. The objective was to enhance the steady-state and transient performance with respect to current, torque, and speed against time when the load torque changes from 0 to 10 Nm using double-cage rotor. The transient characteristics of the machine was demonstrated for no-load, half load, and full load. The simulation revealed that with double-cage rotor, the magnitude of the starting current was reduced while the starting torque was increased under all loading conditions. When a load change of 50% to 100% occurred for load torque of 10 Nm, it was clearly observed that the dynamic of single cage did not adequately fit the electromagnetic torque-speed curve within the 3 s simulation time frame. The simulation time was increased to 10 s as shown by the variation of speed over the range of 0 to 1500 rpm, indicating that only double cage can fit into the curve very well. The analysis indicated that the addition of inner cage has resulted in higher torque and lower resistances during the starting of the motor and improved the transient response time in terms of induction motor's starting performance.*

Keywords— ***Double cage rotor, Induction motor, Load torque, Transient response, Single-cage motor***

1. INTRODUCTION

The conventional single cage induction motor has been widely used in many industrial processes, however its performance suffers from the problem of high starting current and low starting torque, which reduces the running efficiency of motor [1]. As a result of this, the motor in single cage arrangement is not suitable for direct-on-line starting and not useful for starting under heavy load conditions. In addition, there is little evaluation regarding the operation of a motor within safe limit without exceeding the temperature based on the temperature of the rotor. Thus, considering these disadvantages of starting, running and braking under specific conditions inherent in single cage rotor, this paper attempts to address the limitation of fixed torque associated with the constant rotor resistance of a squirrel cage induction machine and the high current surge at start-up that results in reduced running or transient performance efficiency, using double-cage configuration.

The double-cage induction machine can be produced in large numbers in small and large sizes because of its robust construction. With double cage configuration, there is no need maintaining slip rings and brushes, the use of direct-on-line (DOL) starter to start of motor is possible, it is applied when starting under heavy load conditions, and provides good efficiency during running (i.e. transient state) conditions.

There are several researches regarding double cage induction modelling and parameter estimation that studies system performance characteristics. The output characteristics of both single cage and double cage machine have been determined using hybrid simulated annealing-evaporating rate water cycle algorithm (SA-ERWCA) based on their equivalent circuit parameter estimation [2]. The performance of standard induction motor was improved using dual-rotor permanent magnet induction motor (DRPMIM) whose model was established as a two-dimensional finite element model using Maxwell Ansoft software [3]. In order to meet the function of differential mechanism and vehicle drive, electromagnetic differential model of double-rotor induction motor was designed [4]. Parameter estimation using measured resistance and reactance at different frequencies was carried out for squirrel cage induction motor in terms of single-cage model and double-cage model using a phase-to-phase standstill variable frequency test [5]. Dynamic modelling of a series of induction motors squirrel cage with different shapes of rotor deep bars taking into considering the skin effect, with the study showing that double cage motor has the advantage of operating with lower speed due to non-existent unstable region [6]. The magnetic field distribution, electromagnetic performances and equivalent circuit parameters of multiphase double cage rotor inductions in healthy and broken bars condition have been evaluated using analytical method [7]. The advantage of double cage motor over single cage motor in terms of torque-speed and stator current-speed was investigated [8]. The speed control of double cage rotor induction motor for hybrid vehicle was carried out using field oriented vector control [9]. Similarly, indirect vector control of double cage machine was

presented [10]. Analytical method for predicting the transient behaviour of squirrel cage induction motors subjected to pulsating mechanical loads such as a reciprocating compressor was developed [11]. Simulations of induction motors in static and dynamic conditions based on the transient behaviour of the machine was shown through the current, electromagnetic torque, electromagnetic torque versus speed, and speed under no-load, half-load (50%), and full-load (100%) conditions [12].

The ideal conditions for starting induction motors require the following: good supply regulation with low inrush currents, a high starting torque to accelerate the load to its stable operating speed, and a high factor to limit the wattage power for a given load requirement [13]. Hence, the advantage of double-cage rotor over single-cage rotor in providing improved starting torque with reduced starting current is leveraged in this paper by examining the transient behaviour of 37.3 kW induction motor via simulation.

2. MATHEMATICAL MODELLING OF DOUBLE CAGE MOTOR

In order to carry out the mathematical modelling of induction motor in this work, the following is worthy of note: the chosen state variable is the flux linkage. It has been chosen because it provides more stability with the same integration time step in the digital simulation of induction motor model [14], the concept of a rotating d-q field reference (without saturation) assumed for developing induction machine model [15], and the modelling of the double-cage induction machines is carried out using Park transformation in a fixed reference direct axis and quadrature axis (d-q reference frame).

The mathematical derivation of the equations representing the dynamics of double-cage induction machine is performed in a way closely similar to d-q reference frame model of the single-cage induction machine. The addition of second cage results in the rotor being described with four differential equations in the d-q reference axis. The equivalent circuits for the d-axis and q-axis are shown in Fig. 1 and Fig. 2 and are used to derive the mathematical model. Thus, the double-cage induction machine can be analysed in d-q reference axis by adopting the generalized theory of electrical machines [10].

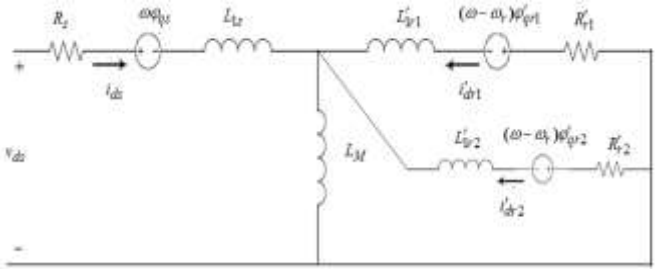

Fig. 1. *Equivalent circuit of double-cage induction machine in d-reference axis*

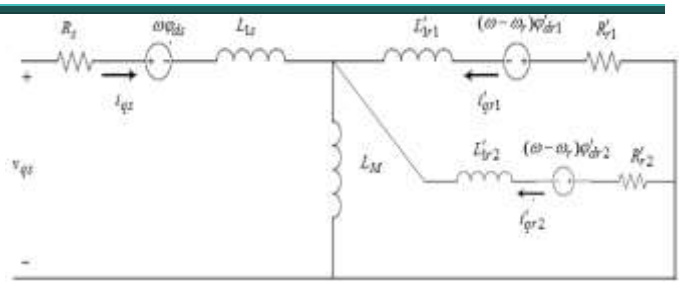

Fig. 2. *Equivalent circuit of double-cage induction machine in q-reference axis*

From Figures 1 and 2, it is assumed that for the double-cage induction machine, the rotor bars are short circuited and thus rotor voltages, v'_{dr1}, v'_{qr1}, v'_{dr2}, and v'_{qr2}, are equal to zero. Hence, the d-axis and q-axis voltages of the stator and rotor sides are given by:

$$v_{qs} = R_s i_{qs} + \omega\varphi_{ds} + d\varphi_{qs}/dt \quad (1)$$

$$v_{ds} = R_s i_{ds} - \omega\varphi_{qs} + d\varphi_{ds}/dt \quad (2)$$

$$0 = R'_{r1} i'_{qr1} + (\omega - \omega_r)\varphi'_{dr1} + d\varphi'_{qr1}/dt \quad (3)$$

$$0 = R'_{r1} i'_{dr1} - (\omega - \omega_r)\varphi'_{qr1} + d\varphi'_{dr1}/dt \quad (4)$$

$$0 = R'_{r2} i'_{qr2} + (\omega - \omega_r)\varphi'_{dr2} + d\varphi'_{qr2}/dt \quad (5)$$

$$0 = R'_{r2} i'_{dr2} - (\omega - \omega_r)\varphi'_{qr2} + d\varphi'_{dr2}/dt \quad (6)$$

The magnetizing flux linkages are defined for the double-cage induction machine by the following equations:

$$\varphi_{qs} = L_{Is} i_{qs} + L_m\left(i_{qs} + i'_{qr1} + i'_{qr2}\right) \quad (7)$$

$$\varphi_{ds} = L_{Is} i_{ds} + L_m\left(i_{ds} + i'_{dr1} + i'_{dr2}\right) \quad (8)$$

$$\varphi'_{qr1} = L'_{Ir1} i'_{qr1} + L_m\left(i_{qs} + i'_{qr1} + i'_{qr2}\right) \quad (9)$$

$$\varphi'_{qr2} = L'_{Ir2} i'_{qr2} + L_m\left(i_{qs} + i'_{qr1} + i'_{qr2}\right) \quad (10)$$

$$\varphi'_{dr1} = L'_{Ir1} i'_{dr1} + L_m\left(i_{ds} + i'_{dr1} + i'_{dr2}\right) \quad (11)$$

$$\varphi'_{dr2} = L'_{Ir2} i'_{dr2} + L_m\left(i_{ds} + i'_{dr1} + i'_{dr2}\right) \quad (12)$$

The mutual flux linkage between the stator and outer cage, the stator and inner cage, and between the outer cage and inner cage can be expressed in terms of the mutual inductance L_m given by:

$$\varphi_{qm} = L_m\left(i_{qs} + i'_{qr1} + i'_{qr2}\right) \quad (13)$$

$$\varphi_{dm} = L_m\left(i_{ds} + i'_{dr1} + i'_{dr2}\right) \quad (14)$$

Equations (1) to (14) describe the dynamics of the double-cage induction machine in the d-q frame.

3. SYSTEM MODEL

In this section, the proposed block diagram of the dynamic model for double cage motor is presented in terms of double cage flux and voltage equations. The physical machine consists of a stationary part (stator) and a rotating part (rotor), both with their own reference frame. Thus, proposed block diagram of double-cage model is shown in Fig. 3.

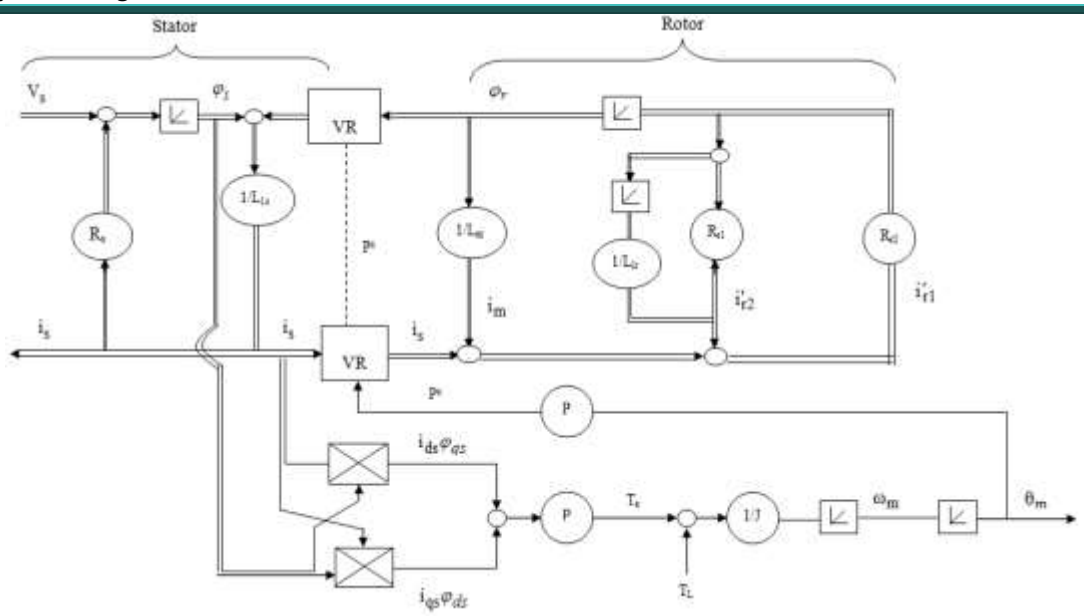

Fig. 3 *Proposed block diagram of double-cage model*

Considering the block diagram in Fig. 3, the following mechanical equations representing the dynamic model of the motor are derived. The mechanical rotation speed given by:

$$\omega_m = \frac{1}{J}\int (T_e - T_L)dt$$

(15)

The mechanical angle is given by:

$$\theta_m = \int \omega_m$$

(16)

The electromagnetic torque is given by:

$$T_e = \frac{3}{2}p\left(\varphi_{ds} i_{qs} - \varphi_{qs} i_{ds}\right)$$

(17)

From Figure 3.6, the stator voltage is given by:

$$v_s = R_s i_s + \dot{\varphi}_s$$

(18)

The total stator flux is given by:

$$\varphi_s = \int (v_s - R_s i_s)dt$$

(19)

The current flowing in the stator circuit is given by:

$$i_s = \frac{\varphi_s - \varphi_{r1}}{L_{ls}}$$

(20)

The outer and inner-cage rotor voltages are given by:

$$0 = R_{r1} i'_{r1} + \dot{\varphi}_{r1}$$

(21)

$$0 = R_{r2} i'_{r2} + \dot{\varphi}_{r2}$$

(22)

The flux due to each double cage is given by:

$$\varphi_{r1} = -\int R_{r1} i_{r1}\, dt$$

(23)

$$\varphi_{r2} = -\int R_{r2} i_{r2}\, dt$$

(24)

The currents flowing in the rotor circuit can be expressed by:

$$i_r = \frac{\varphi_{r1}}{L_m} - i_s$$

(25)

$$i_{r1} = i_r - i_{r2}$$

(24)

$$i_{r2} = \frac{\varphi_{r2}}{L_{lr2}}$$

(25)

Equations (15) to (25) were obtained from the proposed block diagram of the dynamic model shown in Fig. 3. It should be noted that the block diagram in Figure 3 can easily be reduced to a single-cage model by removing the inner loops (that is R_{r2}, L_{lr2}).

The parameters used for the simulation carried out in MATLAB/Simulink environment are shown in Table 1.

Table 1: Motor Parameters

Motor Parameter Definition	***Symbol***	***Value***
Stator resistance	R_s	3.5 Ω

Motor Parameter Definition	*Symbol*	*Value*
Stator reactance	X_s	2.17 Ω
Single cage rotor resistance	R_r	3.16 Ω
Single cage rotor reactance	X_r	2.14 Ω
Outer cage (or cage 1) rotor resistance	R_{r1}	9.3 Ω
Outer cage (or cage 1) rotor reactance	X_{r1}	0.11 Ω
Inner cage (or cage 2) rotor resistance	R_{r2}	8.6 Ω
Inner cage (or cage 2) rotor reactance	X_{r2}	0.65 Ω
Mutual reactance	X_m	81.64 Ω
Line to line voltage	V_n	400 V
Rotor speed	ω_m	1500 rpm
Moment of inertia	J	0.102 Jkg.m^2
Friction coefficient	F	0 N.m.s
Number of poles	*p*	2
Nominal power	P	37.3 kW

4. RESULTS AND DISCUSSION

The machine is fed from a 400 V, 50 Hz supply. The performance analysis of the induction machine has been presented for has been presented in terms of single cage and double cage regarding the transient characteristics of the stator current (or line current), rotor current, torque, speed, and torque versus speed during starting given that the machine is not loaded (that is operating at no load), the machine is 50% loaded (operating at 50% loading), and the machine is 100% loaded (operating at full load) in steady state or constant load case. Also, the machine transient characteristics were examined for dynamic state when the load changes from 50% to 100% loading assuming 5 Nm and 10 Nm load torque.

4.1 Machine at no Load

In this case, 0% load torque was assumed such that mechanical torque T_L 0 Nm was fed to machine. the simulation results of the transient characteristics during starting assuming no loading and with the machine configured as single cage and double cage induction motor are presented in Fig. 4 to 8 for line current (three-phase stator current), three-phase rotor current (cage 1 and cage 2), electromagnetic torque, electromagnetic torque versus speed, and speed respectively.

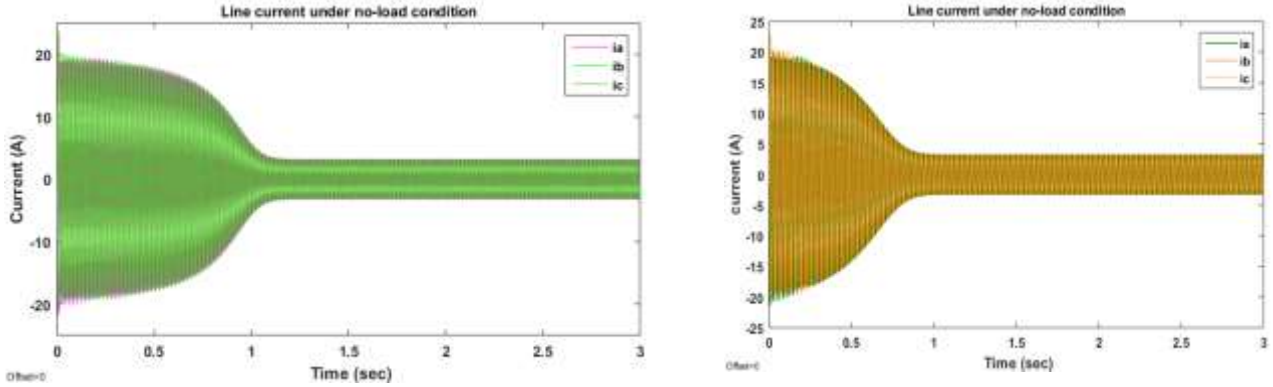

(a) (b)

Fig. 4. *Line (stator) currents under no load: (a) single cage, (b) double cage*

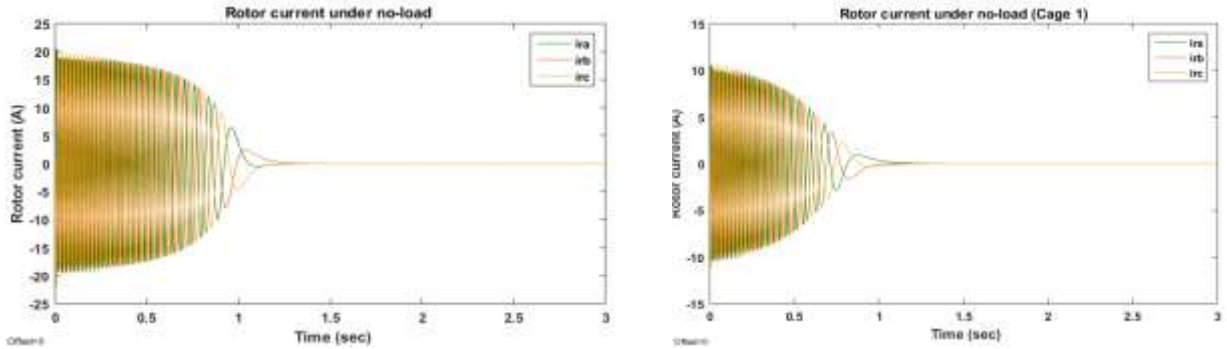

(a) (b)

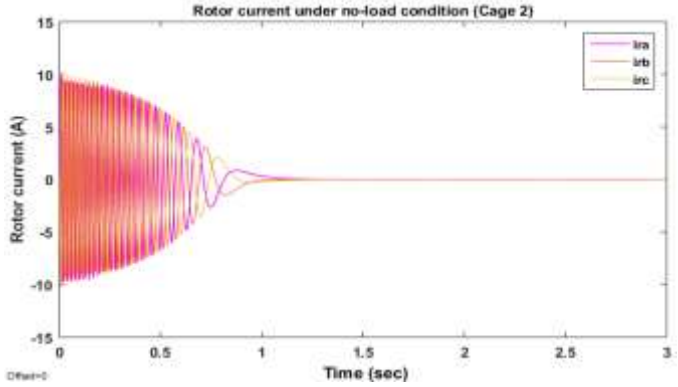

(c)

Fig. 5. *Rotor currents under no load: (a) single cage, (b) & (c) cage 1 and cage 2 (double cage)*

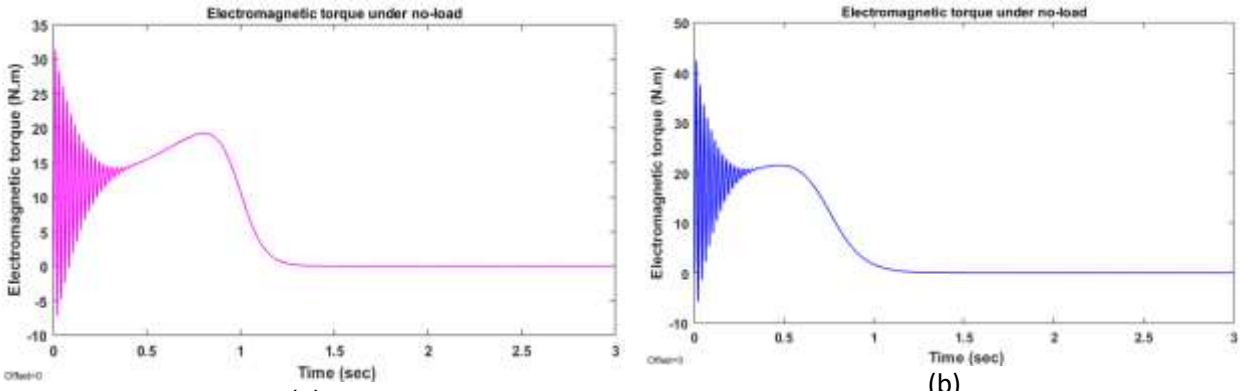

(a) (b)

Fig. 6. *Torque under no load: (a) single cage & (b) double cage*

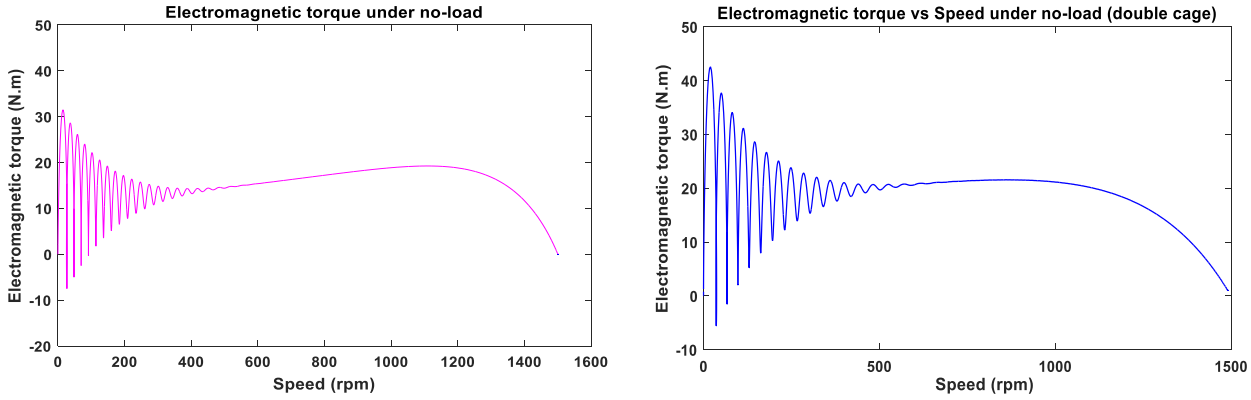

(a) (b)

Fig. 7. *Torque versus speed under no load: (a) single cage & (b) double cage*

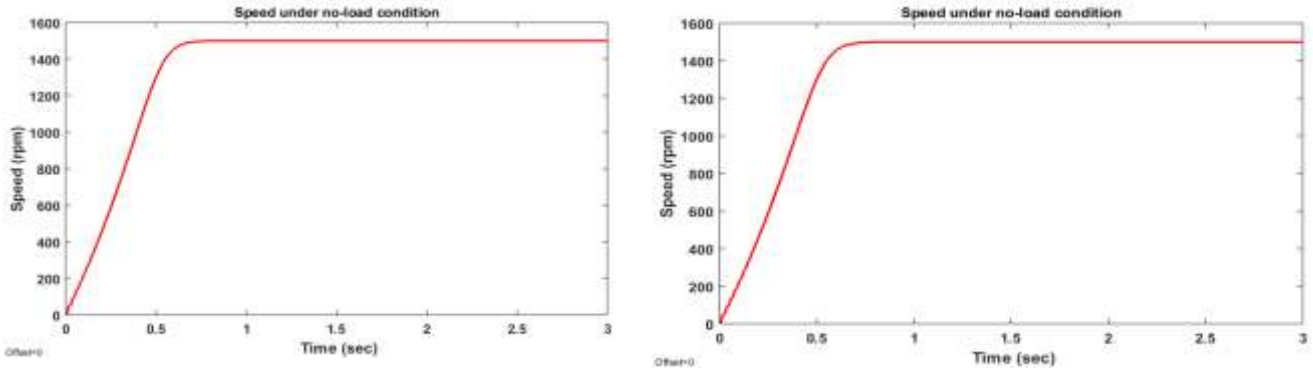

(a) (b)

Fig. 8. *Motor Speed under no load: (a) single cage (b) double cage*

The starting current was initially high but decreases gradually over time as shown in Fig. 4. However, it can be seen that during the starting of the machine, the rotor current for the double cage was less than that of single cage. Whereas the starting current for single cage rotor was 20.2 A as shown in Figure 5a, for the double cage rotor as shown in Fig. 5b and 5c, it was 10.13 A for cage 1 and cage 2 respectively. This is because the current path through the rotor has been splinted in double cage rotor. The electromagnetic torque of the single cage as shown in Fig. 6a oscillates during the transient state and the same holds in the case of the double cage in Fig. 6b, and later the oscillation stops and then proceeds towards the load torque. However, to counter the effect of high starting current with low starting torque common with induction machine, the starting electromagnetic torque in this case was higher for the double cage compared to the single cage. That is 42.5 Nm against 31.38 Nm, which is 35.4% increase in starting torque. The same cycling or oscillation was evident during the transient state with the electromagnetic torque plotted against speed in Fig. 7. But, similar to the single cage, the machine torques terminates at the maximum speed as the machine rated speed (synchronous speed) because of no load effect. Figure 8 also shows a small disturbance in the speed during start-up. This, just like the single cage, is due to the electromagnetic torque oscillation. A steady-state speed is reached, which is equal to the synchronous speed because the machine is unloaded. Generally, the transient behaviour of the double cage motor under no load is that its rise time (time to respond) to input signal was 0.66 s, and settling time (time to settle or reached steady state) was 0.94 s against rise time of 0.81 s and settling time of 1.09 s for single cage motor. Hence, the double cage provides less starting rotor current than single cage rotor and also achieve faster response time including reaching steady-state at approximately 0.15 s faster than the single cage rotor.

4.2 Machine at Half Load

This subsection considers a scenario where the machine is 50% loaded assuming a load torque T_L= 5 Nm was connected to it. The resulting simulation plots for single cage and double cage are presented with respect to 50% loading of the machine. The analysis is presented for line current in Fig. 9, rotor current in Fig. 10, electromagnetic torque in Fig. 11, electromagnetic torque against speed in Fig. 12, and speed in Fig. 13.

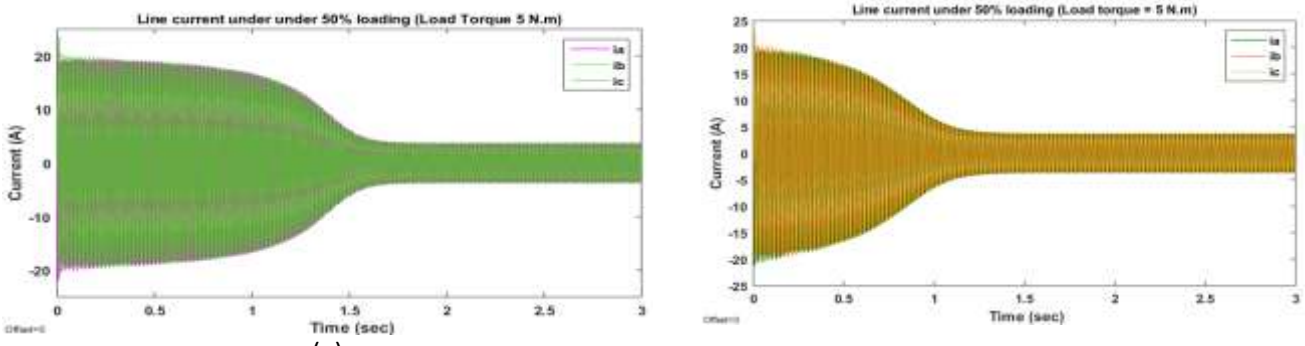

(a) (b)

Fig. 9. *Line (stator) currents under 50% loading: (a) single cage, (b) double cage*

International Journal of Academic Engineering Research (IJAER)
ISSN: 2643-9085
Vol. 8 Issue 5 May - 2024, Pages: 1-10

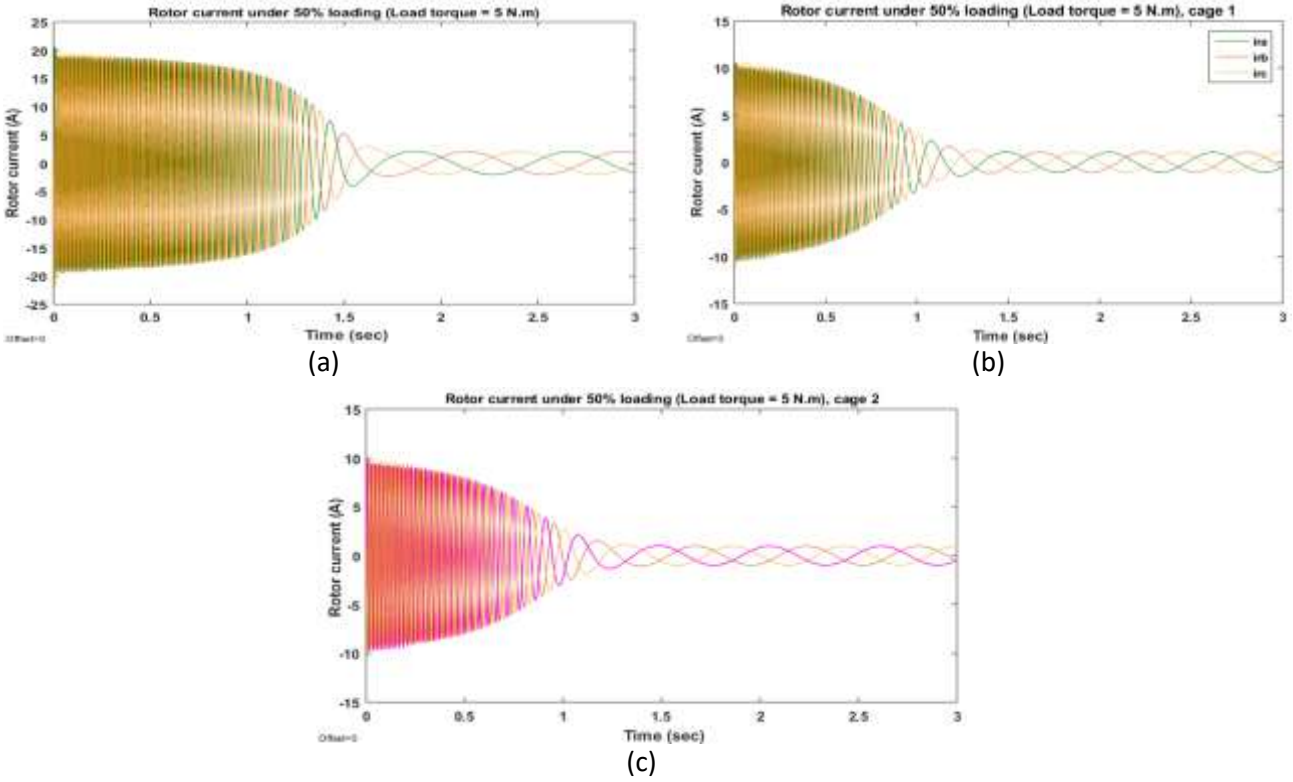

Fig. 10. *Rotor currents under 50% loading: (a) single cage, (b) & (c) cage 1 and cage 2 (double cage)*

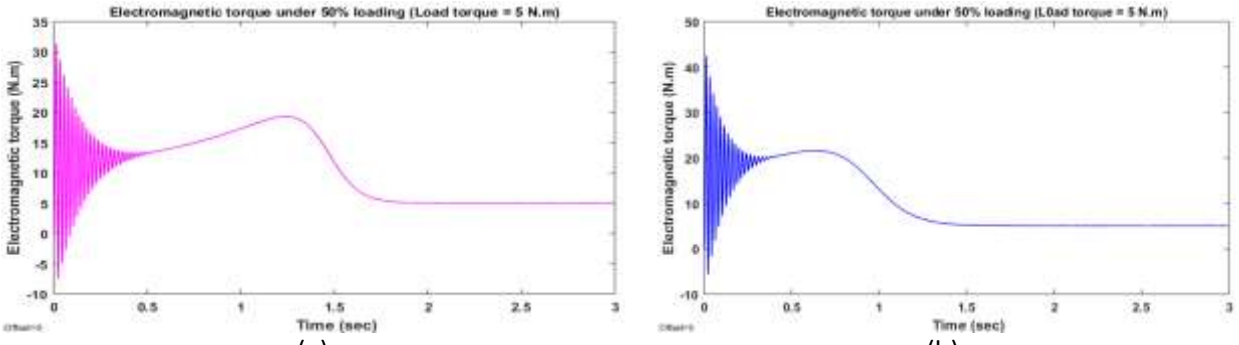

Fig. 11. *Torque under 50% loading: (a) single cage & (b) double cage*

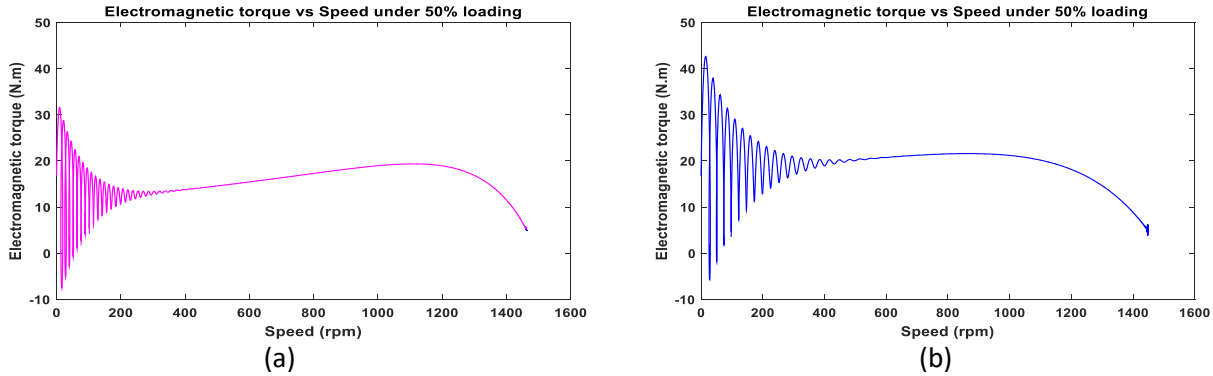

Fig. 12. *Torque versus speed under 50% loading: (a) single cage & (b) double cage*

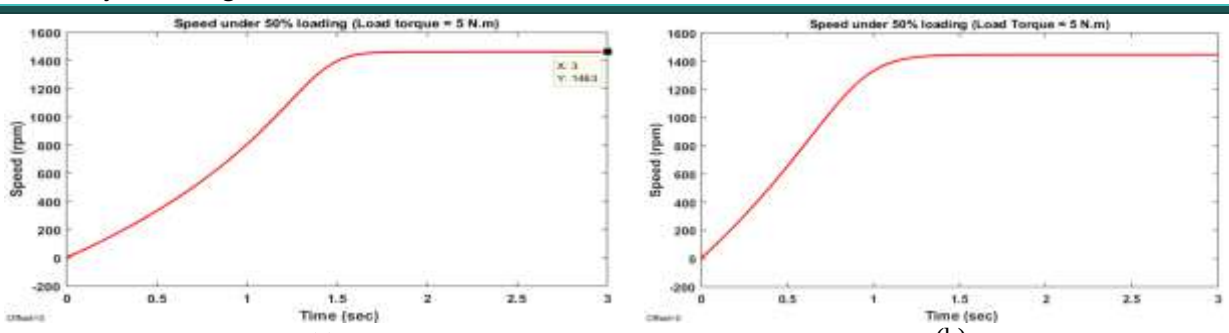

(a) (b)

Fig. 13. *Motor Speed under 50% load: (a) single cage (b) double cage*

As shown in Fig. 9a to 13a, it can be seen that the machine reached the steady-state nearly at 0.5 second later compared with no load condition for the single cage. That is, with connected load torque, the machine takes longer time to reach steady state. This is expected as a result of increase in load torque. Looking at Figures 9 and 10, the amplitude (or magnitude) of both line current and rotor current were not affected by the increased magnitude of the load (torque) for single cage and double cage. Hence, it suffices to say that the machine current is not affected by the external load and it is only a function of the parameters of the machine [12]. As shown in Figure 12, the torque terminates at 5 Nm and at a speed less than the synchronous speed. In Figure 13 the maximum speed attained is lower than with no load.

4.3 Machine at Full Load

Now, simulations are carried out to evaluate the steady-state transient characteristics of the machine as single cage rotor and as double cage rotor motor assuming 100% loading, which is considered a 10 Nm load torque condition. In this case, the steady-state transient characteristics of single cage and double cage model are examined via simulation assuming a load torque 10 N.m (full load or 100% loading). The machine characteristic is presented in terms of line current in Fig. 14, rotor current in Fig. 15, electromagnetic torque in Fig. 16, electromagnetic torque against speed in Fig. 17, and speed in Fig. 18.

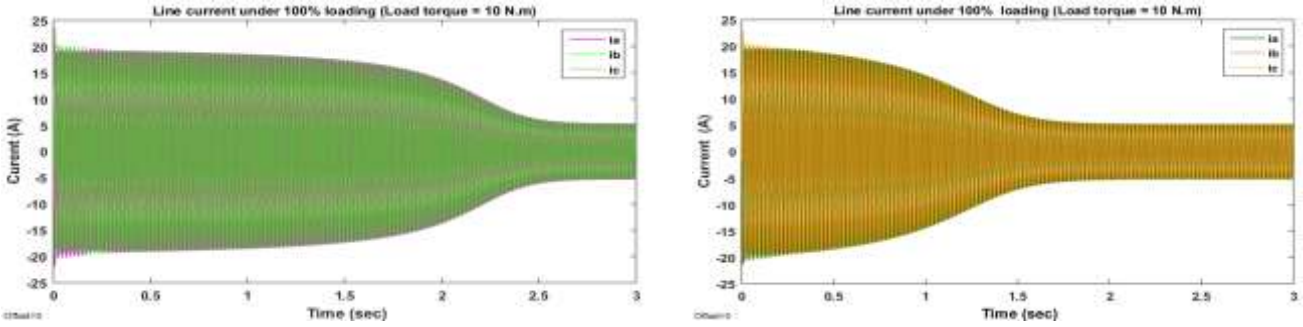

(a) (b)

Fig. 14. *Line (stator) currents under 100% loading: (a) single cage, (b) double cage*

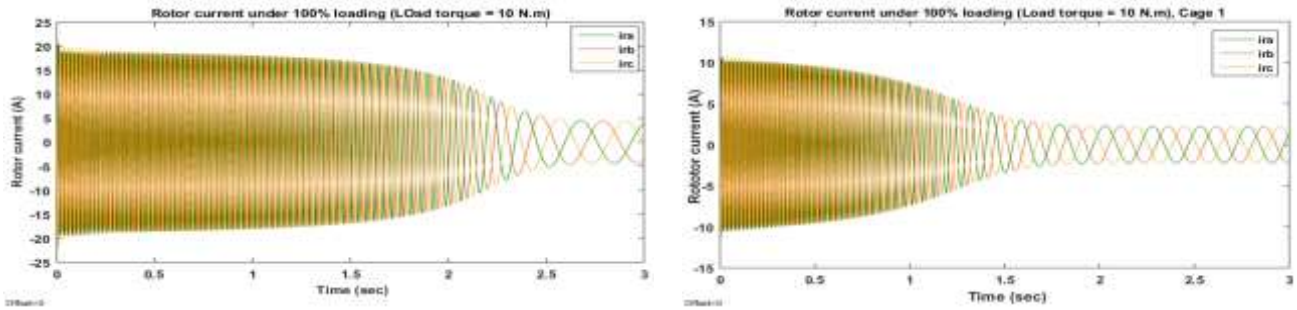

(a) (b)

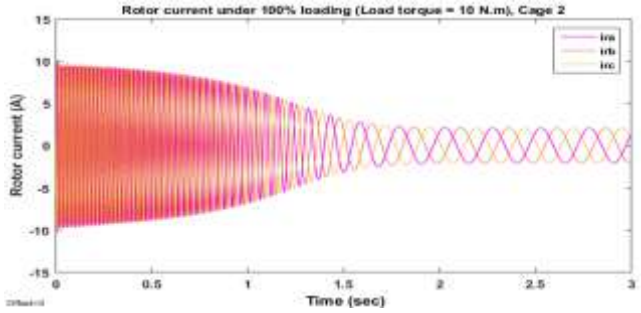

(c)

Fig. 15. *Rotor currents under 100% loading: (a) single cage, (b) & (c) cage 1 and cage 2 (double cage)*

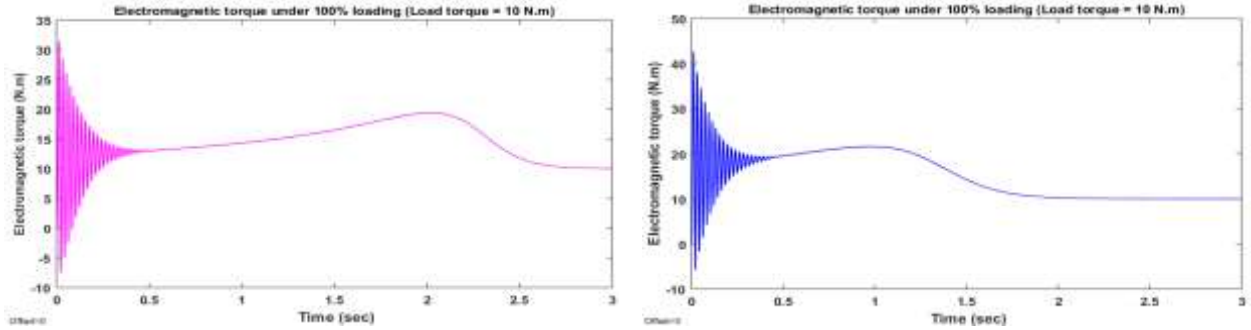

(a) (b)

Fig. 16. *Torque under 100% loading: (a) single cage & (b) double cage*

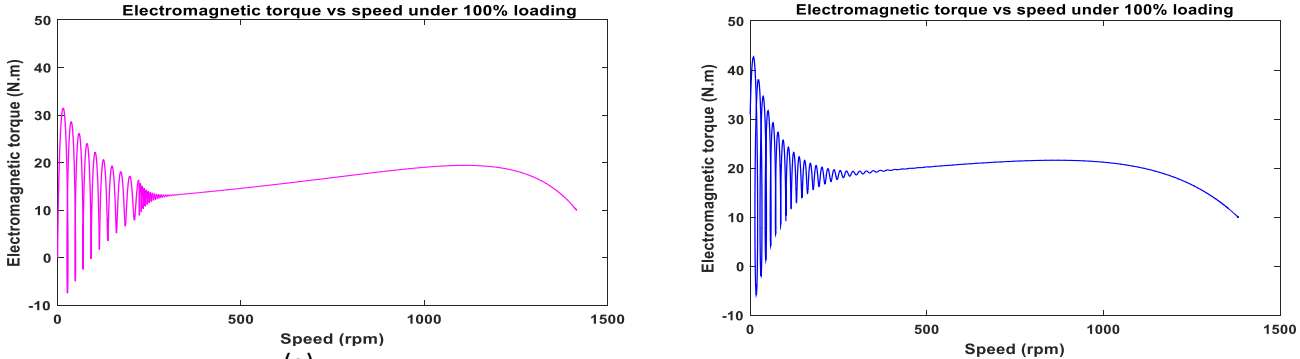

(a) (b)

Fig. 17. *Torque versus speed under 100% loading: (a) single cage & (b) double cage*

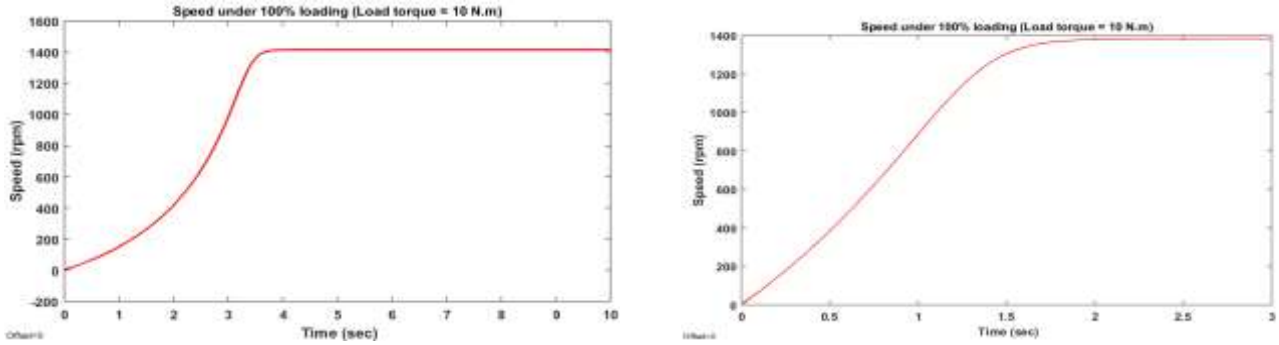

(a) (b)

Fig. 18. Motor Speed under 100% load: (a) single cage (b) double cage

With full load scenario considered (that is 100% load torque), it takes 1.4 s longer for the single cage motor to reach steady-state than with 50% load torque as shown in Figure 14a to17a. Figure 18a revealed that the speed of the single cage machine takes approximately 3.5 seconds to reach steady-state. Thus, this simulation analysis revealed that the single cage machine did not adequately fit into time response curve of the rotor speed within the 3 s simulation-time frame.

In this case, looking at Fig. 14b, 14c, 15b, 16b, and 18b, at full load or 100% loading (assumed as 10 Nm load torque), it can be seen that it takes almost 0.5 second longer for the double cage machine to reach steady-state than during 50% loading (half load). Fig. 18b revealed that the speed of the double cage machine takes 1.69 s to reach steady-state.

5. CONCLUSION

The simulation results have been presented for the steady-state transient characteristics of 37.3 kW three-phase squirrel cage induction motor considering two configurations, single cage rotor and double cage rotor, and basically analysed for no load, 50% loading (half load), and 100% loading (full load) simulation scenarios. Generally, the rate of the voltage induced in the rotor is the same as the rate of the supply at the starting of the motor. It can be seen that the starting currents of the double rotor windings were 10.13 A for both cage 1 and cage 2 respectively and this is less than that of the single cage rotor winding, which was 20.2 A. This means that the single cage rotor has more starting current than double cage rotor. The simulation results indicated that during the starting of the machine, the starting current was initially high but decreases over time, and the same holds for the electromagnetic torque. However, the machine speed increases until an optimal point. The single cage rotor had higher starting rotor current than double cage rotor. On the other hand, double cage rotor motor offers better starting torque than the single cage rotor with reduced starting current. Thus, the simulation revealed that the double cage rotor increased the starting torque by 35.4%. In both the single cage and double cage configurations, the machine reached the synchronous speed under no load case. However, under 50% loading (half load) and 100% loading (full load), the synchronous speeds for both single cage rotor and double cage rotor were 1463/1447 rpm and 1415/1387 rpm. This means that the speed of induction machine is affected by increased load. In addition, the increase in load affects the time it takes for the system to reach steady-state. Besides, the simulations have shown that the double cage rotor reaches steady-state transient optimal value faster than the single cage rotor at full-load.

REFERENCES

[1] Electrical Deck. (2021). Double cage induction motor – Construction, working & advantages. Available online at: https://www.electricaldeck.com/2021/01/double-cage-induction-motor.html?m=1. Access on May 8, 2023.

[2] Ćalasan, M.; M. Micev; Z. M. Ali; A. F. Zobaa and S. H. E Abdel Aleem. (2020). Parameter estimation of induction machine single-cage and double-cage models using a hybrid simulated annealing–evaporation rate water cycle algorithm. Mathematics, 8, Article ID 1024, 1-29.

[3] Diao, T. (2015). Study on dual-rotor permanent magnet induction motor and performance. The Open Electrical & Electronic Engineering Journal, 9, 954-590.

[4] Adamczyk, D.; A. Wilk and M. Michna . (2016). Model of the double-rotor induction motor in terms of electromagnetic differential. Archives of Electrical Engineering, 65 (4): 761-772.

[5] Monjo, L.; F. Córcoles and Pedra, J. (2015). Parameter estimation of squirrel-cage motors with parasitic torques in the torque-slip curve. IET Electric Power Applications, 9 (5): 377-387.

[6] Maddi, Z. and Aouzellag, D. (2017). Dynamic modelling of induction motor squirrel cage for differentshapes of rotor deep bars with estimation of the skin effect. Progress In Electromagnetics Research M, 59, 147-160.

[7] Boughrara, K. and Ibtiouen, R. (2014). Analytical modeling of double cage rotor induction motors in healthy and broken bars conditions. Paper presented at International Conference on Electrical Sciences and Technologies in Maghreb (CISTEM2014), Tunis, Tunisia, 1-8.

[8] Yahaya, E. A.; T. Omokhafe, E. O. Agbachi and A. G. James. (2015). Advantage of double cage rotor over single cage rotor induction motor. Innovative Systems Design and Engineering, 6 (12): 1-4.

[9] Sinchuk, O. and Kozakevych, I. (2019). Control system of double-rotor induction motors for hybrid vehicles. Electrical Complexes and Systems, 2, 72-78.

[10] Guru, N.; S. K. Mishra and B. Nayak. (2013). Indirect vector control of multi cage induction motor. International Journal of Computer Applications, 68 (2): 25-32.

[11] Al Sayari, N. M. (2011). Dynamic analysis of cage rotor induction motor using harmonic field analysis and coupling inductances method. PhD Dissertation, School of Electrical and Electronic Engineering, University of Manchester, UK.

[12] Le Roux, P. F. and Ngwenyama, M. K. (2022). Static and dynamic simulation of an induction motor using Matlab/Simulink. Energies, 15, 3564: 1-21.

[13] Okoro, C. C. (2004). Electrical machines and system, the challenge for a culture of self-reliance. University of Lagos Inaugural Lecture Series, UNILAG Press.

[14] Kumar, S.; P. K. Ghosh and S. Mukherjee. (2011). The d-q modeling, order reduction and numerical analysis of double cage three phase induction machine for power system studies. International Journal of Computer and Electrical Engineering, 3 (2): 303-308.

[15] Idoko, A. A.; I. T. Thuku, S. Y. Musa and C. Amos. (2017). Design of tuning mechanism of PID controller for application in three phase induction motor speed control. International Journal of Advanced Engineering Research and Science, 4 (11): 138 – 146.